1999

Observation and application of optical interference and diffraction effects in reflection from photochemically fabricated Gaussian interfaces

Lynne Koker
University of Birmingham

Kurt W. Kolasinski
West Chester University of Pennsylvania, kkolasinski@wcupa.edu

Observation and application of optical interference and diffraction effects in reflection from photochemically fabricated Gaussian interfaces

Lynne Koker and Kurt W. Kolasinski

Citation: Journal of Applied Physics **86**, 1800 (1999); doi: 10.1063/1.370972
View online: http://dx.doi.org/10.1063/1.370972
View Table of Contents: http://scitation.aip.org/content/aip/journal/jap/86/4?ver=pdfcov
Published by the AIP Publishing

Observation and application of optical interference and diffraction effects in reflection from photochemically fabricated Gaussian interfaces

Lynne Koker and Kurt W. Kolasinski[a)]
School of Chemistry, University of Birmingham, Edgbaston, Birmingham B15 2TT, United Kingdom

(Received 30 November 1998; accepted for publication 10 May 1999)

A HeNe laser has been used to fabricate photochemically a photoluminescent porous Si thin film on top of crystalline Si. The porous Si film has Gaussian shaped upper and lower interfaces. When the reflection of a laser beam from this film during, or after, the photochemical process is observed, two distinct, concentric circular interference patterns are observed. A pattern of thick rings is superimposed upon a pattern of fine rings. The reflected beam is far more divergent than the incident beam. The formation of the outer rings is a coherent phenomenon. Analysis of the patterns indicates that reflection from the upper interface is not involved in the ring formation process but that optical interference and Fresnel diffraction of the light reflected from the bottom interface cause the pattern formation. It is shown that the radius of the pattern is linearly proportional to the optical path length through the film. Therefore, measurements of pattern sizes yield information about the depth and index of refraction of the porous Si film. This observation provides us with a novel, *in situ* technique for measuring the kinetics of formation of the photoluminescent silicon thin films and might be exploited for applications in chemical sensing. © *1999 American Institute of Physics.* [S0021-8979(99)05316-5]

I. INTRODUCTION

Porous silicon (por-Si) has attracted great interest recently not only due to its potential use in optoelectronic devices,[1] but also as a possible substrate for chemical sensors[2] and even as a biomaterial.[3] Porosity superlattices have recently been fabricated that show promising optical properties.[4,5] Lateral superlattices have been formed in por-Si which act as diffraction gratings.[6,7] Therefore, there is great interest in discovering how to control both the fabrication process and the properties of por-Si films. Porous Si is conventionally made by electrochemical etching or by the use of various chemical stain etches.[1,8,9] Studies have shown that photoluminescent Si can be produced photochemically by illuminating crystalline silicon (c-Si) while it is immersed in aqueous hydrofluoric acid (HF(aq))[10–14] or mixtures of HF with nitric acid and water.[15–17]

Thin film interference effects have been observed in a variety of guises, including the observation of ring patterns in reflection. Ring patterns produced by a separated by implanted oxygen layer on silicon (an oxide made by oxygen ion implantation into a Si wafer) have been observed and used to determine the quality of the layer.[18] Similar patterns were reported with thin superconducting films[19] and oil drops.[20,21] The thickness and structure of tear films in mammalian and human eyes have also be been probed using thin film interference techniques.[22–24] In all of these cases, the observed ring patterns have been ascribed solely to interference effects. Insofar as por-Si films are concerned, white light interference effects have been observed in reflection from photochemically produced por-Si.[10,14] In carefully prepared electrochemically grown por-Si, the formation of an optical cavity has been observed.[25] This effect has been exploited in color image generation[26] and to produce an extremely sensitive chemical sensor.[2]

In the course of studies on the photochemical production of por-Si, we observed pattern formation in laser light reflected from these photochemically produced structures. In this article we report on this observation, attempt an analysis of the patterns, and demonstrate that measurements of the patterns can yield information on the depth of the buried por-Si/c-Si interface. We find that the pattern formation does not depend on the presence of the film. The only influence of the film on the patterns is to change the pattern size due to the effects of refraction. The pattern formation process depends intimately on the interplay between interference and Fresnel diffraction of the light reflected from the bottom interface. It is the shape and depth of the lower interface that determine the focusing properties of this interface and it is the combination of the focusing properties and Fresnel diffraction that determine the divergence and, therefore, the size of the reflected beam. Because of this, we are able to show that the pattern size is linearly proportional to the depth of the lower interface.

II. EXPERIMENT

Samples of $\sim 1\ \mathrm{cm}^2$ were cut from n-type Si(111), typically 4.5–6.4 Ω cm. These were immersed in electronics grade aqueous HF (48% w/w unless otherwise stated) and irradiated at near normal incidence with fluences on the order of 1–100 $\mathrm{mW\,mm^{-2}}$ of 632.8 nm light from a HeNe laser. Two different HeNe lasers were employed. Their nominal powers were 0.8 and 15 mW. Both lasers exhibit Gaussian intensity profiles [$I = \exp(x^2/2\sigma)$] but are slightly divergent

a)Author to whom correspondence should be addressed; electronic mail: K.W.Kolasinski@bham.ac.uk

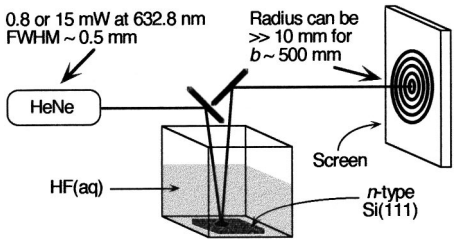

FIG. 1. A schematic illustration of the experimental setup. The distance from the Si crystal surface to the imaging screen is denoted b. For intensity profile measurements the screen is replaced by a photodiode mounted on a translation stage.

with typical full widths at half maximum of roughly 0.5 mm ($\sigma = 0.21$ mm). The reflected beam was studied as the por-Si formed and also after the crystal had been removed from the HF(aq). The por-Si layers are stable in air. The patterns remain qualitatively unchanged over a period of months.

The irradiated areas were examined by a stylus profilometer (Rank Taylor Hobson Form Talysurf 120 L) and TopoSurf three dimensional imaging software. The profilometer allows us to determine both the functional form of the interfaces and their depth. The air/por-Si interface is measured after rinsing and drying the sample. The por-Si is then removed by immersing the silicon in 1 M NaOH for 5–10 min so that we can measure the profile of what had been the por-Si/c-Si interface.

The methods of observing the interference patterns are shown schematically in Fig. 1. We can photograph the pattern formed on a screen placed at a distance b from the surface of the crystal. To measure intensity profiles, the screen is replaced by a photodiode (Si/PIN) mounted on a translation stage. We place a 10 μm pinhole in front of the photodiode to define the lateral resolution. The same photodiode has been used to measure the reflected intensity. The reflected intensity of both the entire beam and the intensity along the center line (using the 10 μm pinhole) have been measured. Unless otherwise stated, all error bars correspond to 1 standard deviation.

III. RESULTS

A. Photochemical interface fabrication

Details of the photochemical production of por-Si are reported elsewhere.[27] In short, we observe that brief irradiation (~30 s) by the HeNe in HF(aq) produces a dark spot on the crystal. The spot grows until, at $t \approx 5$ min, it is the same diameter as the laser beam. When illuminated with a handheld UV lamp (254–366 nm), the spot luminesces with an orange glow when observed in air but green luminescence is observed when the UV illumination is carried out in the HF solution. In contrast to the report of Curtis *et al.*,[25] we do not observe any interference structure superimposed upon PL spectra even though interference patterns are observed in laser beams reflected from the film. This is an indication that simple Fabry–Pérot interference cannot explain the interference patterns we observe. The observation of strong, visible, room temperature PL, in accordance with previous work,[10,13,14] is taken as evidence of the formation of por-Si.

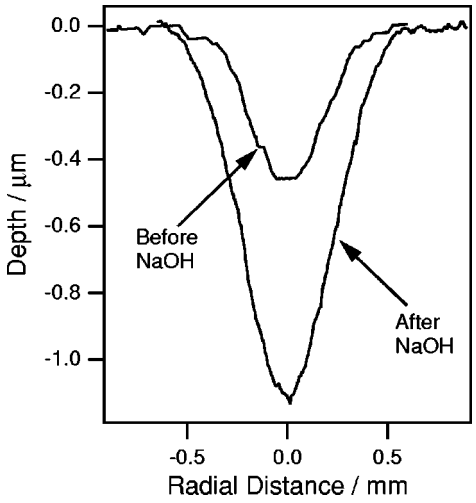

FIG. 2. A profilometer image of a typical film in vertical cross section along the film diameter. Note that the vertical axis is greatly magnified in comparison to the horizontal axis.

Strong visible PL is generally[1] associated with a porosity of roughly 60%–80%. The presence of por-Si is corroborated by the strong Si–H_x absorption peak observed in the Fourier transform infrared spectrum of a freshly prepared spot.

Profilometry results indicate that the photochemical processing leads to a film with Gaussian shaped upper and lower interfaces, an example of which is shown in Fig. 2. This particular film was fabricated with an 0.8 mW HeNe which had a Gaussian intensity profile characterized by $\sigma = 0.225$ mm. The top (air/por-Si) interface is well fitted ($\chi^2 = 0.055$) by a Gaussian with a maximum depth of $d^t_{\max} = 0.470 \pm 0.001\ \mu$m and $\sigma = 0.179 \pm 0.001$ mm. The bottom (por-Si/c-Si) interface is well fitted ($\chi^2 = 0.079$) by a Gaussian with $d^b_{\max} = 1.001 \pm 0.002\ \mu$m and $\sigma = 0.217 \pm 0.001$ mm.

It is found that the depth of the interfaces and the thickness of the film increase with increasing irradiation time. Further, the σ values of the upper and lower interfaces always closely resemble the σ value of the laser used to fabricate the film. This indicates that the film forms only in the irradiated area and that any pattern formed in the laser intensity profile can be transferred to the shape of the film. We have confirmed this by fabricating films of different shapes including a single ring and concentric rings without the aid of a mask, but instead relying only upon the intensity profile of the incident light. Noguchi and Suemune[28] have also demonstrated selective area growth of por-Si structures. Their method attains very high lateral resolution but requires patterning p-doped regions on an n-type Si wafer.

B. Pattern development in time

Immediately after directing the laser onto the crystal, the reflected beam has the intensity profile of the incident beam. A halo of diffuse light develops around the central spot which gradually separates from the central spot and forms a ring around it, leaving a dark circle between the two areas of light. The outer ring and dark circle progressively increase in diameter. A second light ring forms within the dark circle,

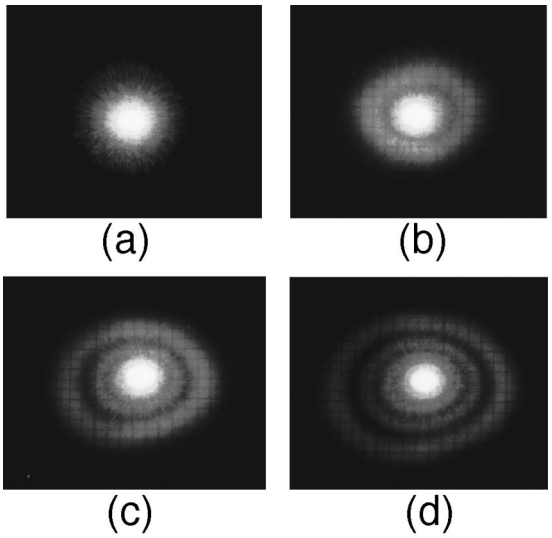

FIG. 3. The temporal evolution of the reflected beam as a Si crystal is irradiated in HF(aq) is followed photographically. The reflected beam was imaged 1 m away from the crystal surface. The time of exposure was: (a) 2 min, (b) 4 min, (c) 6.5 min, and (d) 10 min. The cross hatching of a 2 mm/division grid can be seen in (b)–(d).

which subsequently grows in diameter with time. It typically takes ~30 s for a ring to transform from an indistinct halo attached to the central spot to a distinct ring. This sequence is repeated as subsequent rings form as displayed in Fig. 3. It is also possible to discern fine lines within the rings of the outer pattern. Interference patterns with more than ten rings can be created; a six-ring pattern is shown in Fig. 4(a). The outer pattern is composed of rings that are narrower near the center of the pattern and broader toward the outside. We note also that laser speckle is clearly visible in the interference patterns.

The intensity of the reflected beam has been monitored with a photodiode. During the first 3 min of irradiation, we detect a rapid decrease in intensity along the optical axis of the pattern. Thereafter fluctuations, which increase in period and decrease in aplitude, are recorded. There is no obvious relationship between these fluctuations and the formation of the outer or inner pattern.

Closer examination of the central spot reveals that it, too, contains a ring structure as seen in Fig. 4(b). This inner pattern always forms first. With <1 min of irradiation, a fine dark circle forms towards the outer edge of the spot and then contracts. This process repeats itself, producing a pattern of concentric rings, but in this case the narrower rings are on the outside of the pattern. No correlation is found between the appearance of these rings and the appearance of the outer rings, except that the inner pattern always begins to appear before the outer pattern does. The inner pattern is concentric with the outer pattern as it is forming. An intensity maximum normally occurs at the center of this pattern; however, on infrequent occasions a node is observed at the center.

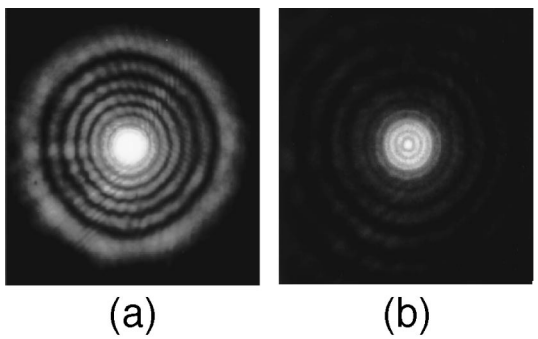

FIG. 4. A pattern ($t_{\text{irradiation}}>30$ min) as imaged in air. Panels (a) and (b) were taken from the same photographic negative at two different exposures to reveal the structure of the inner and outer patterns.

C. Factors that influence the patterns

It is obvious that the patterns grow in size and number of rings as a consequence of the progressively deeper etching of the por-Si film and the broadening (up to a limit) of the spot size. A crucial first observation is that the formation of a pattern does not depend on the presence of the por-Si film. If the film is removed by exposure to a solution of NaOH, the size of the pattern changes but the essential feature of concentric rings is left unmodified.

The visibility of the outer fringes is dependent on the beam quality of the incident laser. The visibility is reduced when the incident beam first passes through a fogged glass plate or a thin piece of plastic. Nonetheless, the pattern still maintains roughly the same diameter (although the edges are made less distinct due to scattered light) and the first few fringes of the inner pattern remain visible. Transmission of the incident beam through plastic or nonclear glass reduces the coherence of the incident light. The effects of beam quality indicate that the outer pattern arises from a phenomenon that depends on the coherence of the incident light, whereas coherence is not a necessary condition for the formation of the inner rings.

IV. DISCUSSION

We now need to determine: (1) why the por-Si film affects the size of the pattern but is not involved in the mechanism of ring formation, (2) why the pattern grows in time, (3) why there appear to be two distinct interference phenomena, (4) why laser coherence strongly affects only one of these interference phenomena, and (5) what affects the size and shape of the pattern. In doing so, we will show that analysis of the patterns can yield information on the refractive index of the film as well as the shape and depth of the lower interface.

A. Effects of the film

First we address how the presence of the film affects the patterns. Since the film is not required for pattern formation, we can immediately rule out any type of amplitude division interference effects (Fabry–Pérot type interference). The reflection from the upper interface (the air/por-Si interface) plays no role in the observed phenomenon. This is not surprising in light of the high porosity of por-Si film. A good approximation of the relationship between refractive index and porosity P is given by the effective medium approximation[29]

$$n=(1-P)n_{\mathrm{Si}}+Pn_{\mathrm{fl}}, \tag{1}$$

where n_{fl} is the index of the fluid in which the por-Si is submerged. A porosity of 80%, therefore, corresponds to an index of 1.58 at 633 nm and a reflectivity at normal incidence of only 0.05. This is an upper bound to reflectivity as the reflectivity at wavelength λ will be attenuated[30] by the rms roughness of the surface Δh by a factor of $\exp(4\pi\Delta h/\lambda)$. Hence the combined effects of porosity and roughness conspire to make the reflection from the upper surface irrelevant to the current problem.

Nonetheless, the presence of the film does affect the size of the pattern. This can be understood as a consequence of refraction. We will demonstrate the quantitative effects of refraction below. For now, it suffices to note that the effect of refractive index on the diameter of the patterns can be checked by placing the crystal in a series of fluids. The outer pattern has a *smaller* diameter and (occasionally) *fewer* rings when the crystal is placed in a fluid with a *low* refractive index, such as air or water, than when compared to a high index fluid such as carbon disulfide. The dependence of the pattern on the por-Si refractive index confirms the effect of refraction and demonstrates that the outer pattern is influenced by the optical path introduced by the por-Si layer.

Lin *et al.*[2] have recently demonstrated a sensitive biosensor based on Fabry–Pérot interference observed in white light reflected from a chemically derivatized por-Si layer. The principle behind this chemical sensing technique is that the binding of molecules at the surface of the por-Si somehow leads to a change in the refractive index of the film. This index change is then observed by changes in the Fabry–Pérot fringes. The effect observed by us can be used in a similar manner as it is also sensitive to changes in the index. The effect reported here may possess several advantages over white light interference. The laser offers high brightness and a collimated light source whose wavelength can be selected to ensure that no photochemistry occurs in the analyte. The effect reported here uses monochromatic light and this makes the use of a spectrometer superfluous for analyzing the patterns.

B. Ray optics of reflection from a Gaussian interface

We now proceed to calculate the image expected for reflection from a film defined by two Gaussian interfaces. Reflection of light from rough[30–38] and curved[20,21,39] interfaces and films has received attention in the literature. We have not, however, found a treatment for reflection from Gaussian shaped interfaces although transmission through Gaussian microlenses has been studied.[40,41] For clarity the macroscopic Si surface will be called the surface and the interfaces of the photochemically treated region will be called the top and bottom interfaces. We assume in all calculations that collimated, monochromatic light is incident upon the surface at normal incidence. The coordinate system is defined in Fig. 5. The idealized film, which grows in the negative z direction, is shown in Fig. 6. We start with the case of reflection from a Gaussian interface in the absence of a film.

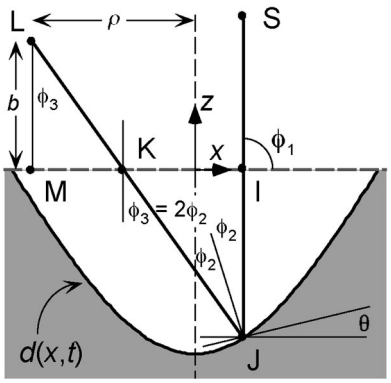

FIG. 5. The notation used to define the cylindrical coordinate system of the optical calculations.

The film has a cylindrically symmetric geometry imparted on it by the laser. As a simplification, we consider the one-dimensional problem along a cord drawn along the film diameter. The radial distance from the center of the spot is x. The depth of the film $d(x,t)$ is centered about $x=0$ and is assumed to be given by the product of two functions. $f(x)$ is the form factor which describes the shape of the interface. $g(t)$ is the growth function which describes the maximum depth of the film as a function of time (the derivative of this function will be denoted as the growth rate). The film grows in the negative z direction. Hence,

$$d(x,t)=f(x)g(t). \tag{2}$$

Referring to Fig. 5, we need to determine the point L on a screen placed a distance b away from the surface of the macroscopic Si crystal for a ray of light that strikes the interface at any arbitrary radial distance x. That is, we need to determine the function $\rho(x,t)$ that describes the radial distance of L from the origin as a function of time. The tangent of $d(x,t)$ determines the effective angle of incidence of the ray which strikes the interface. θ is the angle that the tangent makes with respect to the macroscopic surface. It can be shown by inspection of Fig. 5 that

$$\theta=\tan^{-1}\left(\frac{\partial}{\partial x}d(x,t)\right)=\phi_2, \tag{3}$$

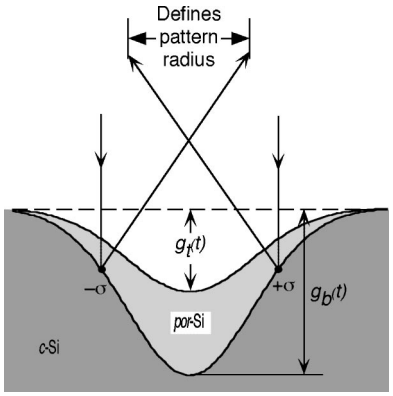

FIG. 6. A ray diagram for reflection from a thin film defined by two Gaussian interfaces. The depth of the film is greatly exaggerated compared to its width.

where ϕ_2 is the angle of incidence on the tangent and $2\phi_2$ is the angle with respect to the surface normal with which the ray leaves the lower interface. The function $\rho(x,t)$ is now found from geometry

$$\rho(x,t)=x-d(x,t)\tan 2\phi_2-b\tan\phi_3. \tag{4}$$

The film has the geometry shown in Fig. 6. The radius of an image is determined by, as will be shown below, the ray which strikes the interface at a distance $x=\pm\sigma$ from the center of the film.

As the interface has been measured to be Gaussian, the form factor is given by

$$f(x)=\exp\left(-\frac{x^2}{2\sigma^2}\right), \tag{5}$$

and, therefore, the derivative of the depth function is

$$\frac{\partial}{\partial x}d(x,t)=-\frac{g(t)x}{\sigma^2}\exp\left(-\frac{x^2}{2\sigma^2}\right). \tag{6}$$

Substitution into Eq. (4) and taking advantage of the small angle approximation ($\tan\phi=\sin\phi=\phi$) yields

$$\rho(x,t)=x+\frac{2g(t)x}{\sigma^2}\exp\left(\frac{-x^2}{2\sigma^2}\right)\left[b+g(t)\exp\left(\frac{-x^2}{2\sigma^2}\right)\right]. \tag{7}$$

The maximum of this function is found by solving the second derivative of the interface profile function. This must be solved analytically but to a close approximation (within 1%), the maximum is found at $x=\pm\sigma$. The radius of an image is then found by substitution for x into Eq. (7)

$$r_{\text{image}}(t)=\sigma+\frac{2b}{\sigma\sqrt{e}}g(t)+\frac{2}{\sigma e}[g(t)]^2. \tag{8}$$

Note that $|g(t)|$ is the maximum depth of the film $d_{\max}$ and that

$$|g(t)|\ll b$$

and

$$|g(t)|\ll\sigma. \tag{9}$$

Therefore, the quadratic term can be neglected. Hence, the image radius for a given depth is given by

$$r_{\text{image}}(t)=\sigma+\frac{2b}{\sigma\sqrt{e}}g(t). \tag{10}$$

Note that the radius as defined is positive in the region from $z=0$ to the focal point and negative beyond the focal point. Since σ is determined by the laser intensity profile and changes little with time, r_{image} increases in direct proportion to the increase in the depth of the interface. Alternatively we can rearrange Eq. (11) to highlight the growth function

$$g(t)=\frac{\sigma\sqrt{e}}{2b}(r_{\text{image}}(t)-\sigma), \tag{11}$$

from which we see that the derivative of $g(t)$, that is the growth rate of the por-Si, is proportional to the slope of a plot of r_{image} vs time.

An inspection of Fig. 6 reveals that the Gaussian interface essentially acts as a focusing mirror. The focal length f_l can be found by setting $r_{\text{image}}=0$, which yields

$$f_l(t)=-\frac{\sigma^2\sqrt{e}}{2g(t)}=\frac{\sigma^2\sqrt{e}}{2d_{\max}}. \tag{12}$$

The focal length, thus, starts at infinity for the flat surface and becomes progressively shorter as the film becomes deeper. For reflection from the bottom interface for the structure shown in Fig. 2 in the absence of the por-Si film, we find $f_l=35.0\pm0.01$ mm. We show below that the change in f_l as a function of depth is crucial for understanding the time development of the patterns.

C. The effect of refraction on reflection from a Gaussian interface

To include the effects of refraction on the image formed for reflection from the bottom interface, is a geometrically straightforward, though algebraically messy, extension of the procedure outlined in Sec. IV B. We start by defining the form factors for the top and bottom interfaces:

$$f_t(x)=\exp\left(-\frac{x^2}{2\sigma_t^2}\right), \tag{13}$$

$$f_b(x)=\exp\left(-\frac{x^2}{2\sigma_b^2}\right). \tag{14}$$

The photochemistry is driven by a laser with an intensity profile of

$$I(x)=I_0\exp\left(-\frac{x^2}{2\sigma_l^2}\right). \tag{15}$$

The profile of the laser beam imparts the geometry of the interface and it has been experimentally verified that we can make the approximation

$$\sigma_l\approx\sigma_t\approx\sigma_b\equiv\sigma, \tag{16}$$

and, therefore,

$$f_t(x)=f_b(x). \tag{17}$$

We then find that the radius of the image formed for reflection from the bottom interface is

$$r_{\text{image},b}(t)=\sigma+\frac{2b}{\sigma\sqrt{e}}[(1-n)g_t(t)+ng_b(t)], \tag{18}$$

where n is the index of the por-Si film. Note that by taking $n=1$, that is for no refraction, the answer for a top interface reflection is retrieved. Furthermore, the observation of a smaller pattern for lower n is consistent with Eq. (18). The growth function of the bottom interface can then be written as

$$g_b(t)=\frac{\sigma\sqrt{e}}{2nb}[r_{\text{image},b}(t)-\sigma]+\frac{(1-n)}{n}g_t(t). \tag{19}$$

D. Intensity profile of reflected beam in the absence of diffraction

Once we have written Eq. (4) and have fixed the distance b to the screen, we are now in the position to calculate the path taken by any arbitrary ray from the laser at S to the screen at point L. As a simplification, we consider only the case in which the film is absent. Equation (4) can be solved numerically. Inspection of the solutions to Eq. (4) reveals that it has one, two, or three solutions in x for a given point on the screen. Each of these solutions corresponds to a ray which can add to the intensity at point L and these ray intensities can be added either coherently or incoherently. This fact forms the basis of the coherence dependence of the outer pattern. We now present the results of both calculations.

The laser beam has a Gaussian intensity profile, Eq. (15). This determines the intensity distribution of the light incident upon the interface at point $d(x,t)$. For three waves of amplitude a_i and phase α_i, the intensity resulting from their combination is

$$I = a_1^2 + a_2^2 + a_3^2 + 2a_1a_2\cos(\alpha_1 - \alpha_2) + 2a_1a_3[\cos(\alpha_1 - \alpha_3) + 2a_2a_3\cos(\alpha_2 - \alpha_3)]. \quad (20)$$

For the incoherent sum, we neglect the cosine terms. For the coherent sum we must know the phase of the three waves. When the source is a laser, the three rays all reach the surface with the same phase; however, they strike the interface at different depths $d(x,t)$. The phase as a function of x can be written

$$\alpha(x) = \frac{2\pi}{\lambda}\{d(x,t) + \sqrt{[b + d(x,t)]^2 + (\rho - x)^2}\} \quad (21)$$

so that the task becomes simply summing up the appropriate intensities for all points L across the diameter of the screen. Note that since the laser intensity profile has a uniform two-dimensional Guassian profile, the interface will also exhibit such a profile and the reflected light will exhibit cylindrical symmetry. In other words, any intensity fluctuations will be observed as rings on a screen. The predicted intensity profiles are shown in Fig. 7(a). Note the sharp cutoff in intensity at a well-defined radius.

These predictions can be compared to the actual intensity profile in Fig. 7(b). We see immediately that the simple reflection model fails miserably to describe the experimental intensity profile. Furthermore, significant intensity is observed beyond the bounds set by the simple reflection model. This is unambiguous proof that diffraction must also be involved in the pattern formation mechanism.

E. Simulation of Fresnel diffraction

The data in Fig. 7 bring us to the conclusion that diffraction must be considered in the pattern formation process. The question immediately arises as to what is causing the diffraction. This is best answered by trying to find a fit to the observed patterns. Wang *et al.*[42] have reported an analytical expression for the radial intensity profile produced by Fresnel diffraction. The reader is referred to the paper of Wang *et al.* for further mathematical details. Fresnel diffraction can best be thought of in terms of Fig. 8. There are four important parameters in determining the intensity distribution as a function of ρ. Once b and λ have been fixed, it is found that R, the source-to-aperture distance, is largely responsible for determining the width of the diffraction pattern, whereas a, the aperture radius, is largely responsible for determining the spacing between successive fringes.

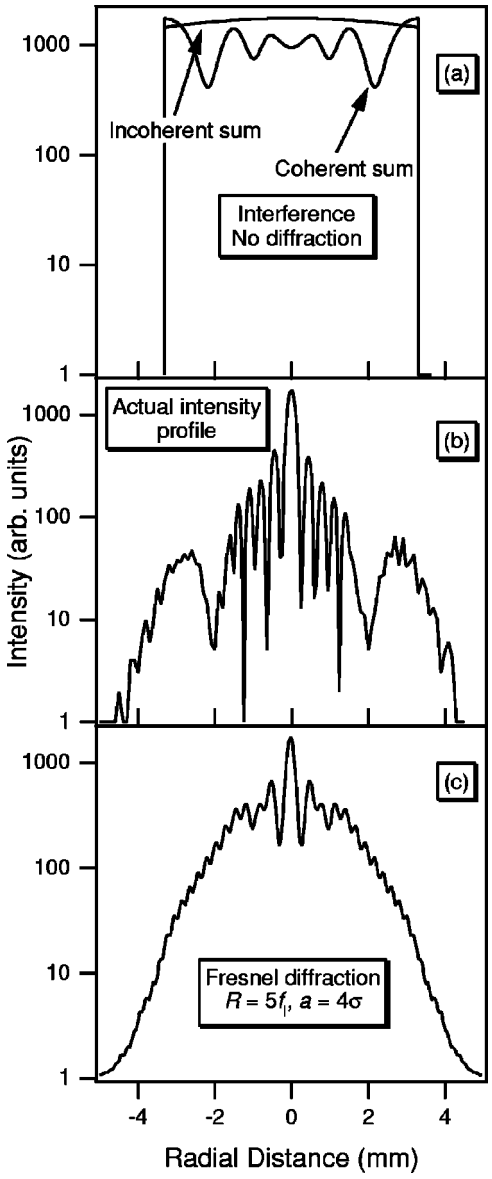

FIG. 7. Radial intensity profiles. For panel (a) the parameters of the interface were taken from the measured profile of the interface shown in Fig. 2 after the por-Si film was removed. The predicted profiles for simple reflection (neglecting diffraction) for incoherent and coherent radiation are indicated. (b) A measured intensity profile. The intensity profile was generated by irradiation of the bottom interface shown in Fig. 2 after removal of the por-Si film. $b = 630$ mm. (c) A simulated Fresnel diffraction pattern. R is set to five times the focal length of the film depicted in Fig. 2 and a is set to 4σ for the same film.

To start the fitting procedure we first consider the aperture size. Either the pore size or the spot size might be considered. The periodicity of the major central fringes is indicative of a spacing that is on the order of the spot radius. Indeed, the simulation shown in Fig. 7(c) assumes a value of $a = 4\sigma$. We see that the fringe spacing is reasonably well

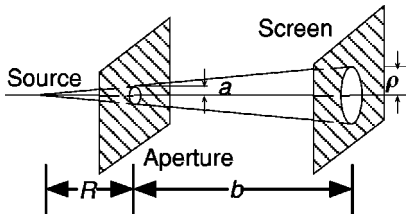

FIG. 8. Schematic diagram of Fresnel diffraction showing the diffracting aperture of radius a, separated from the source by a distance R and the imaging screen by b.

reproduced and we conclude that *the spot size is effectively acting as the aperture size* even though there is no hard aperture in this case (that is, the interface slopes smoothly to the surface level, rather than undergoing a sharp transition).

Second, we consider the source-to-aperture distance. Three alternative come to mind, $R=\infty$ corresponds to a collimated source, that is, it assumes that the source is the laser. If this were the case, the pattern size would not change with time (assuming a fixed aperture size) as the source would be fixed. Simulations also indicate that the pattern is too small compared to the observed profile. The second alternative is that the source should be placed at the bottom interface. This would lead to a pattern that changes with time; however, a retreating source causes the pattern to shrink as the source recedes. Furthermore for $R\sim 1\ \mu$m, the pattern is orders of magnitude too large. The final option is to place the effective source at the focal point of the Gaussian reflector. Our analysis of reflection from a Gaussian interface has shown that the focal length of the reflector decreases as the film gets deeper. The decreasing focal length means that the source is advancing toward the surface and an advancing source leads to a pattern that increases in size as time progresses and the film gets deeper. Therefore, the qualitative trend of increasing pattern size is well reproduced by this choice of the source distance. A simulation run with $a=4\sigma$ and $R=f_l$, however, led to a pattern that is roughly one quarter the size of the measured pattern. Setting $R=5f_l$ reproduces the size of the pattern. This has been done in the simulation shown in Fig. 7(c). No special significance should be given to the factors of 4 and 5 used in this simulation: they simply represent the integer multiplicative factors that lead to the best reproduction of the experimental data.

We conclude that the simplified model of equating the aperture size with the spot size and the source-to-aperture distance with the focal length provides qualitative agreement with our data. The diffraction phenomenon is approximately described by convergent wave Fresnel diffraction. In doing so we can approximate the size of the patterns and the central fringe spacings. We also come to appreciate that the fine structure in the outer rings arises from the low visibility fringes in the outskirts of the Fresnel diffraction pattern. In addition, this treatment makes the proper prediction that the pattern should get larger over time as the film gets deeper. What our simulation fails to reproduce even qualitatively are the distinct outer rings. This is because we have chosen our source to be a point source located near the focal point of the Gaussian reflector. The source term, however, should also account for the coherence of the source [effectively the interference wrinkles displayed in Fig. 7(a)]. Indeed, we have shown in Sec. III C that coherence is important for the formation of the thick outer rings. The overriding contribution to the inner rings, nonetheless, is Fresnel diffraction, which does not require a coherent source. A much more involved treatment of the reflection problem is required to reproduce the diffraction patterns completely accurately.

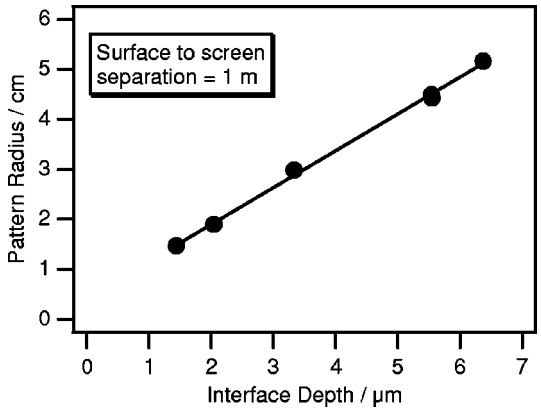

FIG. 9. The dependence of the pattern radius ($b=1$ m) as a function of the maximum depth of the reflecting interface. The depth of the interface was measured after removing the por-Si layer with 1 M NaOH.

F. Application of the diffraction phenomenon to thin film diagnostics

Finally, we demonstrate one application of this newly observed diffraction phenomenon. In Eq. (10), we have shown that the image radius should be linearly proportional to the depth of the lower interface in the absence of the film and neglecting diffraction. Diffraction will change the divergence of the reflected rays but they still propagate rectilinearly. Therefore, we expect that the image radius should still be linearly proportional to the depth of the lower interface but that the constants in the relationship have changed, viz.

$$r_{\mathrm{exp}}(t)=c_0+c_1 d_{\mathrm{max}}(t), \tag{22}$$

where c_0 is related to the size of the laser beam. One consequence of diffraction is that the reflected beam never comes to a focus. Therefore, we write Eq. (22) in an intuitive fashion in which $r_{\mathrm{exp}}(t)$ and $d_{\mathrm{max}}(t)$ are both positive numbers. Both c_0 and c_1 must be determined empirically. In Fig. 9 we plot the measured image radius versus the measured maximum depth of the interface. It is clear that the linear relationship still holds. Therefore, the measurement of pattern radii can be used to determine, at least in relative terms, the depth of interface. This holds out the promise that similar measurements can be applied as an *in situ* probe of the lower interface depth during photochemical processing. We are currently studying this possibility.

V. CONCLUSION

We have reported a novel pattern formation phenomenon in reflected light that occurs during the photochemical fabrication of Gaussian shaped porous Si thin films. We have demonstrated that the effect is due to Fresnel diffraction and

optical interference. We are able to reproduce roughly both the periodicity of the fringe spacing and the size of the pattern by assuming that Fresnel diffraction occurs for a source placed near the focal point of the Gaussian reflector and that the aperture size is roughly equal to the spot size of the structure. We have demonstrated not only that the pattern size depends on the depth of the reflecting interface but also, that if a por-Si film is present above the reflecting interface, the index of refraction of por-Si plays a role in determining the pattern size. These results have two possible practical implications. The first is that measurements of pattern size may be used to measure the depth of the lower interface and, therefore, these measurements may provide the basis for an *in situ* monitor of thin film growth kinetics. The second is that the sensitivity of the pattern size to the index of the film may make the observed diffraction phenomenon a candidate for application in chemical sensing along the lines of the technique demonstrated by Lin *et al.*[2]

ACKNOWLEDGMENTS

L.K. acknowledges the support of the EPSRC through a studentship. The authors are grateful to the Royal Society for the provision of a research grant.

[1] A. G. Cullis, L. T. Canham, and P. D. J. Calcott, J. Appl. Phys. **82**, 909 (1997).
[2] V. S.-Y. Lin, K. Motesharei, K.-P. S. Dancil, M. J. Sailor, and M. R. Ghadiri, Science **278**, 840 (1997).
[3] L. T. Canham *et al.*, Mater. Res. Soc. Symp. Proc. **452**, 579 (1997).
[4] M. G. Berger, C. Dieker, M. Thönissen, L. Vescan, H. Lüth, H. Münder, W. Theiß, M. Wernke, and P. Grosse, J. Phys. D **27**, 1333 (1994).
[5] L. Pavesi, Riv. Nuovo Cimento **20**, 1 (1997).
[6] A. V. Alexeev-Popov, S. A. Gevelyuk, Y. O. Roizin, D. P. Savin, and S. A. Kuchinsky, Solid State Commun. **97**, 591 (1996).
[7] G. Lérondel, R. Romestain, J. C. Vial, and M. Thönissen, Appl. Phys. Lett. **71**, 196 (1997).
[8] R. L. Smith and S. D. Collins, J. Appl. Phys. **71**, R1 (1992).
[9] L. A. Jones, G. M. Taylor, F.-X. Wei, and D. F. Thomas, Prog. Surf. Sci. **50**, 283 (1995).
[10] N. Noguchi and I. Suemune, Appl. Phys. Lett. **62**, 1429 (1993).
[11] Z. Zhang, M. M. Lerner, T. Alekel III, and D. A. Keszler, J. Electrochem. Soc. **140**, L97 (1993).
[12] K. W. Cheah and C. H. Choy, Solid State Commun. **91**, 795 (1994).
[13] C. H. Choy and K. W. Cheah, Appl. Phys. A: Mater. Sci. Process. **61**, 45 (1995).
[14] O. K. Andersen, T. Frello, and E. Veje, J. Appl. Phys. **78**, 6189 (1995).
[15] W. B. Dubbelday, D. M. Szaflarski, R. L. Shimabukuro, S. D. Russell, and M. J. Sailor, Appl. Phys. Lett. **62**, 1694 (1993).
[16] L. A. Jones, Ö. Yükseker, and D. F. Thomas, J. Vac. Sci. Technol. A **14**, 1505 (1996).
[17] D. Dimova-Malinovska, M. Tzolov, N. Malinowski, T. Marinova, and V. Krastev, Appl. Surf. Sci. **96–98**, 457 (1996).
[18] T. Ogawa, L. Taijing, and K. Toyoda, Jpn. J. Appl. Phys., Part 2 **30**, L1393 (1991).
[19] Z. H. Mai, D. Y. Dai, R. L. Wang, H. R. Yi, C. A. Wang, H. C. Li, T. J. Lu, L. Li, and T. Ogawa, J. Mater. Sci. **29**, 3702 (1994).
[20] L. H. Tanner, Opt. Laser Technol. **10**, 125 (1978).
[21] L. H. Tanner, J. Phys. D **12**, 1473 (1979).
[22] D. G. Green, B. R. Frueh, and J. M. Shapiro, J. Opt. Soc. Am. **65**, 119 (1975).
[23] J. I. Prydal, P. Artal, H. Woon, and F. W. Campbell, Invest. Ophthalmol. Visual Sci. **33**, 2006 (1992).
[24] J. I. Prydal and F. W. Campbell, Invest. Ophthalmol. Visual Sci. **33**, 1996 (1992).
[25] C. L. Curtis, V. V. Doan, G. M. Credo, and M. J. Sailor, J. Electrochem. Soc. **140**, 3492 (1993).
[26] V. V. Doan and M. J. Sailor, Science **256**, 1791 (1992).
[27] L. Koker and K. W. Kolasinski, J. Phys. Chem. B (to be published).
[28] N. Noguchi and I. Suemune, J. Appl. Phys. **75**, 4765 (1994).
[29] D. A. G. Bruggeman, Ann. Phys. (Leipzig) **24**, 636 (1935).
[30] J. Szczyrbowski, J. Phys. D **11**, 583 (1978).
[31] J. Musilová and I. Ohlídal, J. Phys. D **25**, 1131 (1992).
[32] I. Filiński, Phys. Status Solidi B **49**, 577 (1972).
[33] I. Ohlídal, F. Lukeš, and K. Navrátil, Surf. Sci. **45**, 91 (1974).
[34] T. Pisarkiewicz, T. Stapinski, H. Czternastek, and P. Rava, J. Non-Cryst. Solids **137–138**, 619 (1991).
[35] F. Carreño, J. C. Martínez-Antón, and E. Bernabeu, Rev. Sci. Instrum. **65**, 2489 (1994).
[36] I. Ohlídal, K. Navrátil, and F. Lukeš, J. Opt. Soc. Am. **61**, 1630 (1971).
[37] J. C. Martínez-Antón and E. Bernabeu, Opt. Commun. **132**, 321 (1996).
[38] J. M. Eastman, in *Physics of Thin Films*, edited by G. Hass and M. H. Francombe (Academic, New York, 1978), Vol. 10, p. 167.
[39] A. González-Cano and E. Bernabéu, Appl. Opt. **32**, 2292 (1993).
[40] R. Grunwald, S. Woggon, R. Ehlert, and W. Reinecke, Pure Appl. Opt. **6**, 663 (1997).
[41] R. Grunwald, S. Woggon, U. Griebner, R. Ehlert, and W. Reinecke, Jpn. J. Appl. Phys., Part 1 **37**, 3701 (1998).
[42] P. Wang, Y. Xu, W. Wang, and Z. Wang, J. Opt. Soc. Am. A **15**, 684 (1998).